NASA

Technical Memorandum 80335

The Dynamics of Oceanic Fronts. Part I The Gulf Stream

Timothy W. Kao

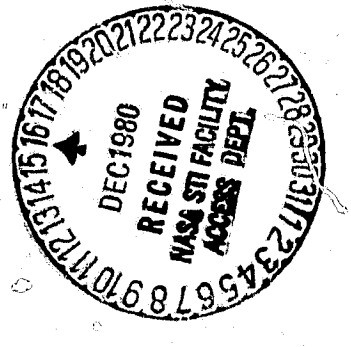

AUGUST 1979

National Aeronautics and Space Administration

Goddard Space Flight Center
Greenbelt, Maryland 20771

TM 80335

THE DYNAMICS OF OCEANIC FRONTS. PART I

THE GULF STREAM

Timothy W. Kao
Laboratory for Atmospheric Sciences (GLAS)

August, 1979

GODDARD SPACE FLIGHT CENTER
Greenbelt, Maryland 20071

THE DYNAMICS OF OCEANIC FRONTS

PART I THE GULF STREAM

Timothy W. Kao*
Laboratory for Atmospheric Sciences (GLAS)

ABSTRACT

The establishment and maintenance of the mean hydrographic properties of large scale density fronts in the upper ocean is considered. The dynamics is studied by posing an initial value problem starting with a near surface discharge of buoyant water with a prescribed density deficit into an ambient stationary fluid of uniform density. The full time-dependent diffusion and Navier-Stokes equations for a constant Coriolis parameter are used in this study. Scaling analysis reveals three independent length scales of the problem, namely a radius of deformation or inertial length scale, L_o, a buoyancy length scale, h_o, and a diffusive length scale, h_ν. Two basic dimensionless parameters are then formed from these length scales; the thermal (or more precisely, the densimetric) Rossby number, $\tilde{R}o = L_o/h_o$ and the Ekman number, $E = (h_\nu/h_o)^2$. The governing equations are then suitably scaled and the resulting normalized equations are shown to depend on E alone for problems of oceanic interest. Under this scaling, the solutions are similar for all $\tilde{R}o$. It is also shown that $1/\tilde{R}o$ is a measure of the frontal slope. The governing equations, in the form used in a previous paper by Kao, et al (1978b), are solved numerically and the scaling analysis is confirmed. The solution indicates that an equilibrium state is established. The front can then be rendered stationary by a barotropic current from a larger scale along-front pressure gradient. In that quasi-steady state, and for small values of E, the main thermocline and the inclined isopycnics forming the front have evolved, together with the along-front jet. Conservation of potential vorticity is also obtained in the light water pool. The surface jet exhibits anticyclonic shear in the light water pool and cyclonic shear across the front. The cross-front ageostrophic circulation is responsible for the maintenance of the front. It is also shown that horizontal diffusive effects are unimportant. Comparisons with known hydrographic features of the Gulf Stream are made, showing superb agreement. It is thus seen the mean Gulf Stream dynamics is indeed a solution of the Navier Stokes and diffusion equations.

For large values of E, it will be shown that another type of scaling is required. That result will be shown in a subsequent paper as Part II of this series, and is relevant to the study of density and current structure on the east coast continental shelf of North America from Newfoundland to Chesapeake Bay, a region subject to forcing by freshwater river discharges.

*Permanent address: Dept. of Civil Engineering, the Catholic University of America, Washington, D.C. 20064.

CONTENTS

TABLES

LIST OF ILLUSTRATIONS

THE DYNAMICS OF OCEANIC FRONTS

PART I THE GULF STREAM

I. INTRODUCTION

Large scale oceanic fronts are pseudo-permanent features of the ocean, often representing the boundaries of water masses of different densities. The lighter water mass is bounded below by the base of the main oceanic thermocline. The isopycnics in the main thermocline are tilted upwards to form the inclined lateral boundary or the front between the light water and the denser ambient water. There is therefore strong horizontal density change across the front. Obviously the horizontal scale of the frontal structure is much smaller than the larger scale of the water masses. Associated with the structure of the density anomaly is a geostrophic current along the front. The boundary currents on the western part of ocean basins are in fact such currents. A prominent example is the Gulf Stream in the North Atlantic. The lighter water in that case is provided by the Sargasso Sea. The inclined isopycnics of the density anomaly, i.e. the front, is sometimes referred to as the "wall" of the Gulf Stream. The isopycnics tilt upwards from the main thermocline at a slope which averages approximately 1:100. Clearly, it is the pressure gradient due to the buoyancy of the lighter water that is the immediate cause of the Gulf Stream. It was also observed (see Stommel, 1966) that the potential vorticity is a constant in the light water. Based on these two concepts, Stommel (see 1966) gave an inviscid, steady-state inertial theory of the Gulf Stream with a two-layer model. This simple model gave a good estimate for the upper ocean transport of the Gulf Stream but failed to produce the shape of the surface jet and over-estimated the maximum velocity of the current. To be sure, the model contained no information on the structure of the Gulf Stream. Later elaborations of the steady-state inertial theory by Charney (1955) and Morgan (1956) incorporated the effects of the change of the Coriolis parameter, f, with latitude and the Sverdrup transport from the interior ocean basin.

In the present paper we investigate the dynamics of establishment and maintenance of the structure of oceanic fronts such as the Gulf Stream. The formation and maintenance of the Sargasso Sea is not addressed in that it is a part of the larger scale dynamics. The dynamics is studied by posing an initial value problem, starting with a near surface flow of light water arising from the

interior ocean basin of Q_0 per unit length into a stationary ambient denser fluid of uniform density ρ_0. When equilibrium is established the frontal structure advances steadily, except for a weak inertial period oscillation. A barotropic current resulting from a larger scale along-front pressure gradient can be superposed to render the front stationary. This will concomittantly render the total vertically integrated cross-front transport to near zero. It will be shown that the quasi-steady density and current structure of the front, obtained as solutions of the full Navier-Stokes and diffusion equations, possess a certain similarity property when proper scalings are used. The scaling analysis is at the heart of the present paper. Comparisons of the present results with the known hydrographic properties of the Gulf Stream are made. Excellent agreement is found. The results therefore elucidate the dynamics of the mean hydrography of the Gulf Stream.

The inflow of buoyant surface water into an ambient stationary fluid has been subject to previous investigations by Kao, et al (1977, 1978a, b), hereafter referred to as I, II, and III. We shall first summarize the physical understanding that we have gained in these studies.

(i) A surface density current whose front advances with a constant speed U_d is established in time $\sim T_1$ ($T_1 \ll 1/f$). The driving force due to buoyancy is balanced at this stage by frictional drag. The detailed distribution of the isopycnics in the current depends only on the Reynolds number Re, ($Re = Q_0/\nu$ where ν is the kinematic viscosity).

(ii) For times less than $1/f$ the effect of the earth's rotation is largely negligible. Thus in estuarine plumes whose time of persistence is less than half of a semi-diurnal tidal period, the frontal structure is well-represented by the results without the earth's rotation as given in I and in Garvine (1974) for the Connecticut River plume reported by Garvine and Monk (1974).

(iii) For longer times, the effect of the earth's rotation becomes increasingly more important. It becomes the dominant factor in time $\sim 2\pi/f$ as shown in III. The development of the along-front current calls into action the Coriolis force which gradually relieves the frictional force from its role in the balance of forces against the driving force of buoyancy. The forward speed of the front is greatly diminished and the structure tends toward a state of geostrophic balance.

This is as far as we went in our previous studies. Rigorous scaling considerations and detailed accounting of the relevance of the model to oceanographic events were not undertaken. In the present paper, we first give the proper scaling laws. It is found that the problem is governed by a

thermal (or densimetric) Rossby number $\tilde{R}o$ and an Ekman number E. Furthermore, for sufficiently small values of E, a normalization can be found so that the solution is similar for all $\tilde{R}o$ and depends on E only. Results of the quasi-steady solution for a small E value are then given.

A recent paper by Garvine (1979) on the steady-state frontal dynamics should be mentioned. Garvine used the momentum-integral technique, familiar in the engineering literature, by prescribing the density field and the shape of the velocity profiles. The prescribed cross-front velocity profile has a surface discharge towards the front and a return flow at greater depth. The flow is assumed to be two-dimensional. Empirical interfacial friction and transport factors were assumed. The frontal shape and the along front velocity at the interface were then calculated. While the present study of frontal dynamics, within the framework of the full dynamical and thermodynamical equations, supports Garvine's assumed surface discharge towards the front as a necessary ingradient for the maintenance of the front, the basis for Garvine's assumption on the role of the interfacial stress is less apparent. The vertical Ekman number is a more natural parameter for measuring the effect of friction than Garvine's scaling parameter Pr based on the interfacial stress coefficient. Indeed, in Garvine's limit for small friction, $Pr \to \infty$, the conservation of potential vorticity in the light water side of the front was not obtained, whereas such a conservation is required by the dynamics.

II. SCALING AND GENERAL CONSIDERATIONS

We begin the scaling analysis by re-stating the initial value problem. A flow near the surface of Q_e per unit length discharges into an ambient stationary fluid of density ρ_o. The inflow has a density deficit relative to the ambient of $(\Delta\rho)_e$. The viscosity of the fluid is ν_e and the Schmidt number is assumed to be unity. The local Coriolis parameter is denoted by f and g denotes the gravitational acceleration. The reduced gravity is g' with $g' = g\,(\Delta\rho)_e/\rho_o$. From Q_e and g' we form a buoyancy velocity scale U_d, $U_d = (g' Q_e)^{1/3}$ and a buoyancy length scale h_o, $h_o = (Q_e^2/g')^{1/3}$. The buoyancy time-scale (short time) is then T_1, $T_1 = h_o/U_d$. From f we form an inertial time scale T, $T = {}^1/f$, and an inertial length scale L_o, $L_o = U_d/f$. A diffusive length scale h_ν is formed from ν_e and f, namely $h_\nu = (\nu_e/f)^{1/2}$. Therefore there are three independent length scales to the problem L_o, h_o and h_ν. These combine to form the two dimensionless parameters of the problem, i.e. the thermal or densimetric Rossby number $\tilde{R}o$,

$$\tilde{R}o = \frac{L_o}{h_o}$$

and the Ekman number, E,

$$E = \left(\frac{h_\nu}{h_o}\right)^2$$

(Note that $\tilde{R}o/E = Re$, the Reynolds number, where $Re = U_d\ h_o/\nu_e$)

We let x* be the horizontal cor-ordinate pointing opposite to the inflow direction and z* be the vertical co-ordinate measured upwards from the free surface. The flow is assumed to be independent of the third co-ordinate y*. Let (u*, v*, w*) be the velocity components in the (x*,y*,z*) directions. We now proceed to scale the problem. We let $(\xi, \eta) = (x^*/L_o, z^*/h_o)$ $\tau = t^*f$ where t* is the dimensional time, and $(\tilde{u}, \tilde{v}, \tilde{w}) = (u^*, v^*, \tilde{R}o\ w^*)/U_d$. The equation of continuity is then

$$\frac{\partial \tilde{u}}{\partial \xi} + \frac{\partial \tilde{w}}{\partial \eta} = 0 \tag{1}$$

If the dimensionless stream function is $\tilde{\Psi}$, $(\tilde{\Psi} = \Psi^*/Q_o)$, then

$$u = \frac{\partial \tilde{\Psi}}{\partial \eta},\ w = -\frac{\partial \tilde{\Psi}}{\partial \xi}. \tag{2}$$

We let the y* - component of the vorticity be ζ^*, i.e., $\zeta^* = \partial u^*/\partial z^* - \partial w^*/\partial x^*$. On normalizing ζ^* by U_d/h_o we get, on using (2),

$$\zeta = (\tilde{R}o)^{-2}\ \frac{\partial^2 \tilde{\Psi}}{\partial \xi^2} + \frac{\partial^2 \tilde{\Psi}}{\partial \eta^2} \tag{3}$$

If we define the density anomaly as γ, $\gamma = (\rho - \rho_o)/\rho_o$ and $\gamma_e = (\Delta\rho)_e/\rho_o$, we can write the normalized anomaly as,

$$\tilde{\gamma} = \gamma/\gamma_e \tag{4}$$

The governing equations are now:

$$\frac{\partial \tilde{\gamma}}{\partial \tau} + \frac{\partial}{\partial \xi}(\tilde{u}\,\tilde{\gamma}) + \frac{\partial}{\partial \eta}(\tilde{w}\,\tilde{\gamma}) = E\left[(\tilde{R}o)^{-2}\ \frac{\partial^2 \tilde{\gamma}}{\partial \xi^2} + \frac{\partial^2 \tilde{\gamma}}{\partial \eta^2}\right], \tag{5}$$

representing the diffusion equation,

$$\frac{\partial \tilde{\zeta}}{\partial \tau} + \frac{\partial}{\partial \xi}(\tilde{u}\,\tilde{\zeta}) + \frac{\partial}{\partial \eta}(\tilde{w}\,\tilde{\zeta}) - \frac{\partial \tilde{v}}{\partial \eta} = \frac{\partial \tilde{\gamma}}{\partial \xi} + E\left[(\tilde{R}o)^{-2}\ \frac{\partial^2 \tilde{\zeta}}{\partial \xi^2} + \frac{\partial^2 \tilde{\zeta}}{\partial \eta^2}\right], \tag{6}$$

representing the Navier-Stokes equation governing the y − component of the vorticity, and

$$\frac{\partial \tilde{\zeta}}{\partial \tau} + \frac{\partial}{\partial \xi}(\tilde{u}\tilde{\zeta}) + \frac{\partial}{\partial \eta}(\tilde{w}\tilde{\zeta}) + \tilde{u} = E\,(\tilde{R}o)^{-2}\frac{\partial^2 \tilde{\zeta}}{\partial \xi^2} + \frac{\partial^2 \tilde{\zeta}}{\partial \eta^2}\,, \tag{7}$$

representing the equation of motion for the $\tilde{v}$− component of velocity. Equations (5), (6), (7) and (3) constitutes the complete set of equations.

(The appropriate manner in which the non-rotating limit is to be viewed is outlined in Appendix B. It is seen that there the approach to steady-state is not uniform for $\tilde{R}o \to \infty$. Thus for any non-zero rotation rate, f, however small, the steady-state solution for large times does not approach the non-rotating limit. The non-rotating solution is however applicable for an intermediate time range $T_1 < t^* < {}^1/_f$).

For most problems of oceanographic interest $\tilde{R}o$ is large, say of the order of 10^2 or larger. (We shall presently see that ${}^1/\tilde{R}o$ is in fact a representative slope of the frontal structure.) Thus we arrive at the result that the dynamics of the frontal structure is similar for all $\tilde{R}o$ and depends on the value of E only. This is so for all stages of the evolution of the frontal development. Indeed for $\tilde{R}o$ large the equations reduce to

$$\frac{\partial \tilde{v}}{\partial t} + \frac{\partial(\tilde{u}\tilde{v})}{\partial \xi} + \frac{\partial(\tilde{w}\tilde{v})}{\partial \eta} = E\frac{\partial^2 \tilde{v}}{\partial \eta^2} \tag{8}$$

$$\frac{\partial \tilde{\zeta}}{\partial t} + \frac{\partial(\tilde{u}\tilde{\zeta})}{\partial \xi} + \frac{\partial(\tilde{w}\tilde{\zeta})}{\partial \eta} - \frac{\partial \tilde{w}}{\partial \eta} = \frac{\partial \tilde{v}}{\partial \xi} + E\frac{\partial^2 \tilde{\zeta}}{\partial \eta^2} \tag{9}$$

$$\frac{\partial \tilde{v}}{\partial t} + \frac{\partial(\tilde{u}\tilde{v})}{\partial \xi} + \frac{\partial(\tilde{w}\tilde{v})}{\partial \eta} + \tilde{u} = E\frac{\partial^2 \tilde{v}}{\partial \eta^2} \tag{10}$$

$$\zeta = \frac{\partial^2 \tilde{\Psi}}{\partial \eta^2} \tag{11}$$

If we admit that the horizontal eddy coefficient $(\nu_e)_H$ is greater than $(\nu_e)_V$ (the vertical eddy coefficient), it is clear that the similarity in $\tilde{R}o$ is still preserved unless $(\nu_e)_H/(\nu_e)_V > (\tilde{R}o)^2$. This is highly unlikely to occur in the scale of motions that we are considering.

We now return to show that ${}^1/\tilde{R}o$ is in fact the representative slope of the front. This is easily shown to be a consequence of the thermal wind balance or Margules Law. Indeed from Margules Law for the limit of vanishing viscosity, we have

$$\Delta v^* = \frac{g \dfrac{(\Delta\rho)_e}{\rho_o}}{f} \cdot s$$

where s = frontal slope, and Δv^* is the across front geostrophic velocity difference. Upon non-dimensionalizing the above, we have

$$\Delta \tilde{v} = \tilde{R}o\, s.$$

We recall that the current was for short times $t^* < 1/f$ in force balance and was travelling at a steady speed U_d. This is thus an inertial current being turned by the earth's rotation. At the new equilibrium state $\Delta v^* \sim U_d$ or $\Delta v \sim 1$. Thus

$$s \sim 1/\tilde{R}o$$

We therefore expect that the frontal slop will have a universal shape in the (ξ, η) co-ordinate independent of $\tilde{R}o$ at any fixed t after quasi-geostrophic equilibrium has been achieved, when Equation (6) reduces to

$$-\frac{\partial \tilde{v}}{\partial \eta} = \frac{\partial \tilde{\gamma}}{\partial \xi}$$

in the region where viscosity is unimportant, i.e. away from the surface Ekman layer. We anticipate such a characterization of the slope to be valid for small values of E, $E \ll 1$. As E increases the region for which this characterization is valid decreases. At large values of E, $E \gg 1$, the frontal structure is predominantly influenced by frictional effect. That case is of interest in the study of shelf-water density and circulation structures and will be investigated in Part II of the present series. It will be shown that another type of scaling law exists for that flow régime.

It is also of interest to examine the vertical component of absolute vorticity, ω^*, where $\omega^* \equiv \frac{\partial v^*}{\partial x^*} + f$. Upon normalization by U_d/h, we have

$$\omega = \frac{1}{\tilde{R}o}\frac{\partial v}{\partial \xi} + 1$$

On differenting Equation (7) with respect to ξ and using the continuity equation, we get in the limit of vanishing viscosity,

$$\frac{\partial \omega}{\partial \tau} + \tilde{u}\frac{\partial \omega}{\partial \xi} + \tilde{R}o\ \tilde{w}\frac{\partial \omega}{\partial \eta} + \frac{\partial \tilde{w}}{\partial \xi}\frac{\partial \tilde{v}}{\partial \eta} + \omega\frac{\partial \tilde{u}}{\partial \xi} = 0 \tag{12}$$

For a region where $\frac{\partial \tilde{v}}{\partial \eta} = 0$, $\frac{\partial \omega}{\partial \eta}$ is easily seen to be also zero and the above equation reduces to

$$\frac{\partial \omega}{\partial \tau} + \tilde{u}\frac{\partial \omega}{\partial \xi} + \omega\frac{\partial u}{\partial \xi} = 0 \tag{13}$$

If such a region exists, and we will show in our initial value problem that it does, let us denote by D its dimensionless vertical extent. We then write the continuity equation as

$$\frac{\partial u}{\partial \xi} + \frac{1}{D}\frac{dD}{dt} = 0 \tag{14}$$

where $\frac{d}{dt} \equiv \frac{\partial}{\partial \tau} + \tilde{u}\frac{\partial}{\partial \xi}$. Combining Equations (13) and (14) then yields the classical law of conservation of potential vorticity

$$\frac{d}{dt}\left(\frac{\omega}{D}\right) = 0$$

We thus see that the law of conservation of potential vorticity is contained in the present formulation. This law together with the thermal wind balance is shown in the paper as a result of the initial value problem in the limit of small viscosity. Thus the simple classical concept of the steady non-linear inertial theory of the Gulf Stream as given in Stommel is embedded in the present framework.

III. DISCUSSION OF RESULTS

1. Similarity and the Approach to Equilibrium

Calculations were made using the formulation and numerical scheme given in III, to confirm the scaling laws, to investigate the approach to quasi-steady equilibrium, and to give the density and current structure of the front. The relationship between the present normalized quantities and the corresponding quantities in the computational formulation is shown in Appendix A. In the actual numerical calculations, every term of the governing equations was, of course, included.

Five cases were computed as summarized in Table I. The range of $\tilde{R}o$ is between 10 and 210 and E is between 0.025 and 2.10. Cases 1 and 2 are identical in E but different in $\tilde{R}o$ and

Table I
Parametric Regime of Computed Cases.

Case No.	$\tilde{R}o$	E
1 (72C)	26.06	0.25
2 (81C)	10.0	0.25
3 (80C)	10.0	0.025
4 (82C)	26.06	0.052
5 (78C)	210.0	2.10

Cases 2 and 3 are identical in $\tilde{R}o$ but different in E. Cases 4 and 5 differ in both $\tilde{R}o$ and E from every other case.

The passage towards quasi-steadiness of the motion of the front is illustrated in Figure 1 where the front speed $\tilde{U}_f$ is plotted against the dimensionless time τ. The movement of the front undergoes a rapid deceleration in the first inertial day. The adjustment towards geostrophy is essentially completed at the end of this duration. This was already shown in III. Subsequent to this initial but primary adjustment, the speed of the front undergoes damped oscillations of inertial frequency. The rate of damping depends on E. In Figure 1 the solid curve is for E =0.025 while the dotted curve is for E = 0.25, i.e. a ten-fold increase in viscosity. Concomitant with the horizontal motion of the front, the frontal structure is deepening, as it must for mass conservation. The rate of deepening is also undergoing damped oscillations with inertial frequency but with opposite phase to the horizontal motion. Quasi-geostrophy is maintained in the frontal region away from the Ekman layer. At any time after the initial adjustment to geostrophy the shape of the inclined bounding isopycnic of the front, beneath the Ekman layer, is universal in the $(\xi_\alpha, \eta_\alpha)$ co-ordinates, defined by $(\xi, \eta)/\alpha$, where α is a constant of propotionality dependent only on the time. The bounding isopycnic of the front is defined here by 1/10 of the total density anomaly $(\Delta\rho)_0/\rho_0$. This is shown in Figure 2 for the five cases listed in Table I at $\tau = 7$ with $\alpha = \pi$. It is seen that the shape is indeed universal.

FRONT SPEED VS TIME: APPROACH TO QUASI-STEADINESS

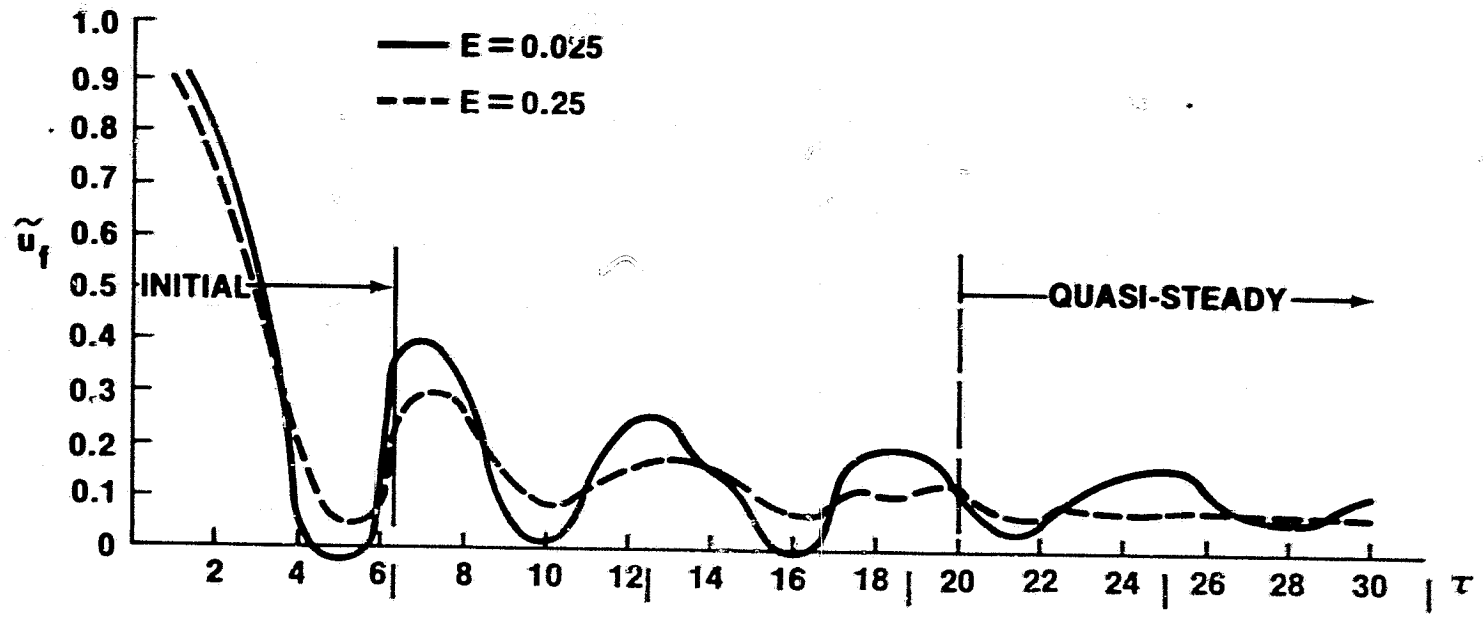

Figure 1. Front Speed vs. Time. Approach to Equilibrium.

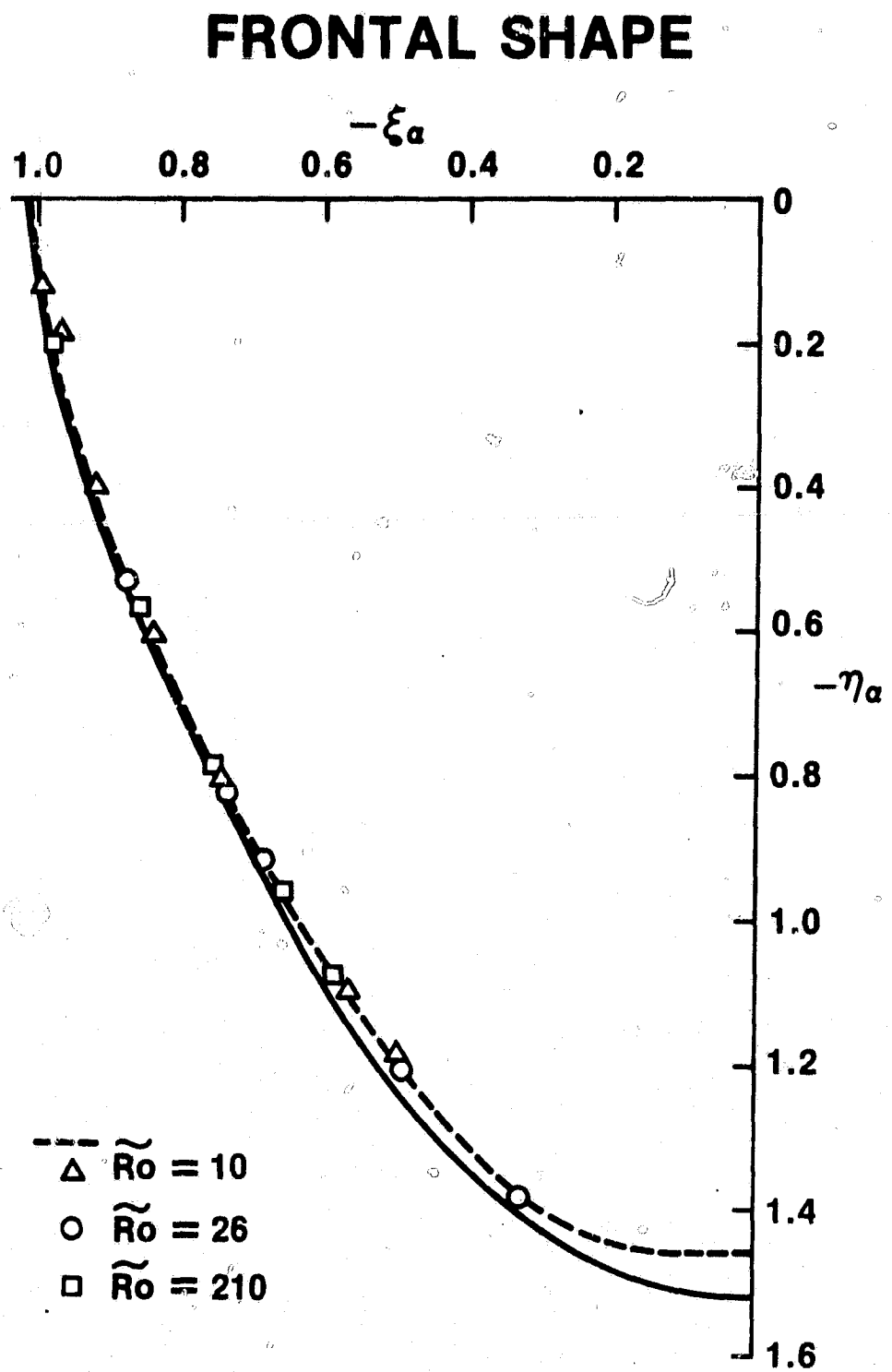

Figure 2. Frontal Shape of different $\tilde{Ro}$, showing similarity in $\tilde{Ro}$.

For the larger values of E, the Ekman layer is relatively thick and is not exhibited in the Figure. For $E \ll 1$, the Ekman layer thickness is small. The dashed line is the shape for $E = 0.025$. For that value of E, it is seen that the mean slope h/L of the bounding isopycnic is equal to $1.5\ h_o/L_o$, or $h/L = 1.5\ /\tilde{R}o$, where h and L are the vertical and horizontal projections of the inclined bounding isopycnic at any time. Thus $h = 1.5\ \alpha\ h_o$ and $L = \alpha L_o$. Furthermore, this mean slope and the shape of the bounding isopycnic is preserved at a later time when quasi-steadiness is approached. The solid line in Figure 2 shows the shape at $\tau = 30$ (with $\alpha = 2\pi$). It is seen that the solid and dashed line are almost coincident over its entirety. If we denote the asymptotic values at equilibrium by an overbar, we then have $\bar{h} = 1.5\ \bar{\alpha} h_o$ and $\bar{L} = \bar{\alpha}\ L_o$ so that $(\bar{h}/\bar{L})$ remains approximately equal to $1.5/\tilde{R}o$ for $E = 0.025$.

At any time after the initial adjustment to geostrophy, the structural features of the front, such as the distribution of the isopycnics forming the front, are found to depend only on E. For example, Figure 3 shows the surface manifestations of the density anomaly across the front for $E = 0.025$ and 0.25. They remain nearly identical for different values of $\tilde{R}o$. Thus the scaling arguments advanced in the previous section are indeed borne out by the results of the actual calculations. In addition, for small values of E, the features become not overly sensitive even to changes in E. For example a change of E from 0.025 to 0.052 (case 4 of Table I) produces almost no change in the structure of the surface density anomaly. For larger values of E however, Figure 3 shows clearly that the compactness of the isopycnics at the front is governed by E. In general, increased vertical diffusion, as represented by the increase in E, causes a broadening of the isopycnics and a thickening of the Ekman layer.

The dynamics of establishment of equilibrium that emerges is really rather simple; namely after the initial primary adjustment to geostrophy, the shape of the frontal boundary in the $(\xi_\alpha, \eta_\alpha)$ – plane is universal away from the Ekman layer and is form-preserving in time. The front undergoes damped inertial period oscillations tending towards an equilibrium state when the deepening of the light water pool is restricted from below. The forward motion of the front

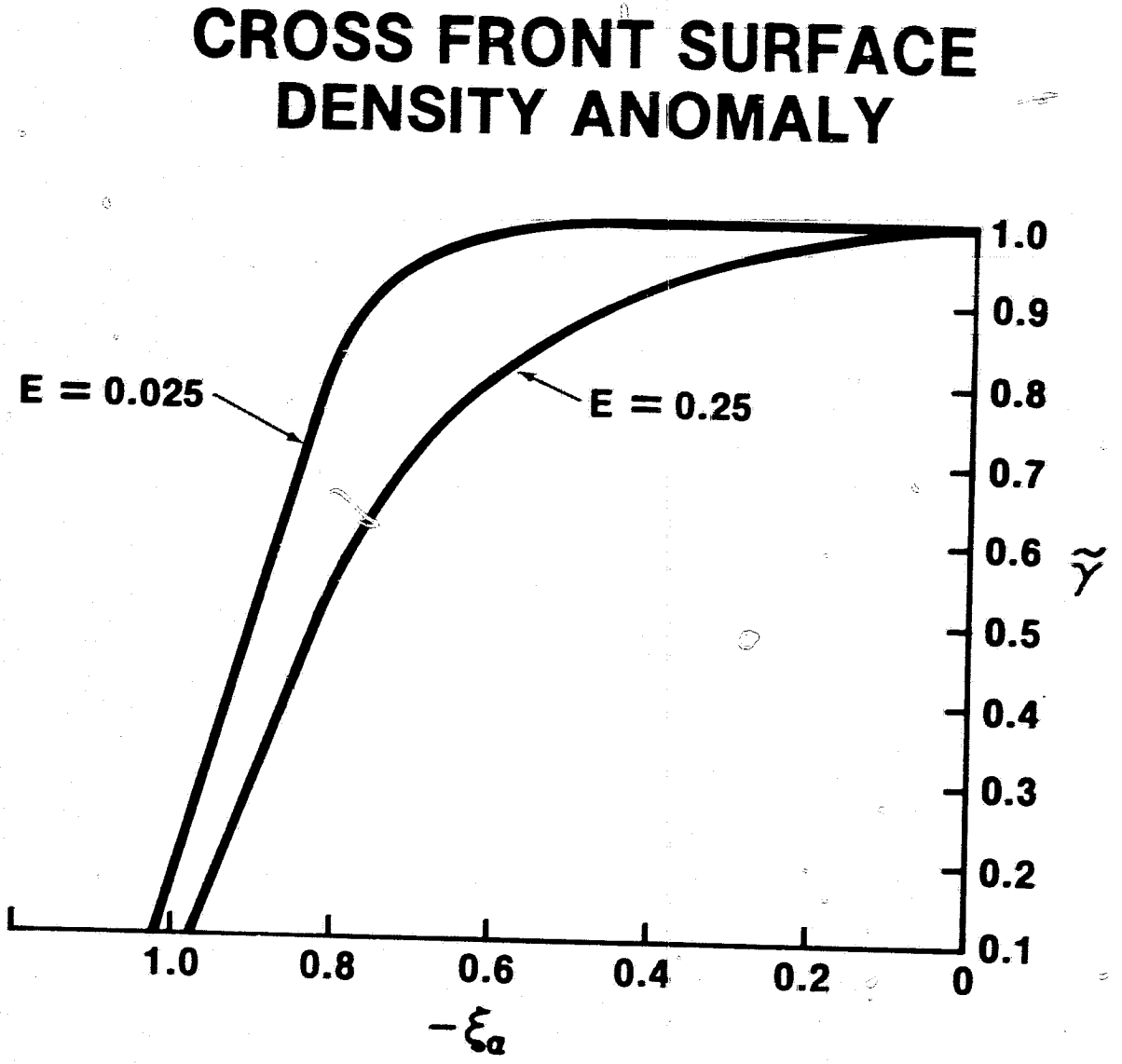

Figure 3. Cross Front Surface Density Anomaly.

in the equilibrium state can be brought to zero by adding a barotropic geostrophic flow resulting from an along front pressure gradient of a larger scale motion. The structure of the front in the quasi-steady state depends only on E. Furthermore, for $E \ll 1$, the structure is even insensitive to changes in the value of E.

We now proceed to discuss the features of the quasi-steady solution for $E = 0.025$. In the next Section we will show that this case gives all the principal features of the mean hydrography of the Gulf Stream.

2. The Quasi-Steady Solution and the Structural Features of the Front

The quasi-steady cross-sectional features of the frontal structure in the vertical plane is summarized and shown in Figure 4. The Ekman Number E is 0.025 and the solution is similar for all $\tilde{R}o$'s. The outstanding feature is the compactness of the inclined isopycnics which form the front and the presence of a pool of light water of almost uniform density. The three dark solid lines are the isopycnics representing 10%, 50% and 90% of the total density anomaly between the incoming light water and the ambient fluid. (Hereafter we shall call them the 0.1, 0.5 and 0.9 isopycnics). To be more specific in terminology we define the region bounded by the vertical at $\xi_{\bar{\alpha}} = 0$ to the 0.1 isopycnic to be the frontal region. The part of the region of almost homogeneous light water bounded by the 0.9 isopycnic is the light water pool. The set of isopycnics between the 0.1 to 0.9 isopycnics, representing 80% of the total density anomaly, will be called the front. At $\xi_{\bar{\alpha}} = 0$, all the isopycnics become horizontal and the vertical extent bounded by the 0.1 and 0.9 isopycnics gives the thickness of the main thermocline. We shall take the 0.9 isopycnic at $\xi_{\bar{\alpha}} = 0$ to be the base of the main thermocline. In Figure 4 the dashed curves are the isotachs of the along-front geostrophic current velocity $\tilde{v}$. The maximum difference in $\tilde{v}$ across the front is 2.0 with the maximum occuring just inside the light water pool. The along front current forms a jet with cyclonic horizontal shear and strong vertical shear in the front, but anticyclonic horizontal shear and no vertical shear in the light water pool. Also shown in Figure 4, as represented by thin solid lines, are the instantaneous streamlines of the cross-front or lateral transport in a frame of reference in which the front is stationary. The streamlines show surface convergence towards the front, down-

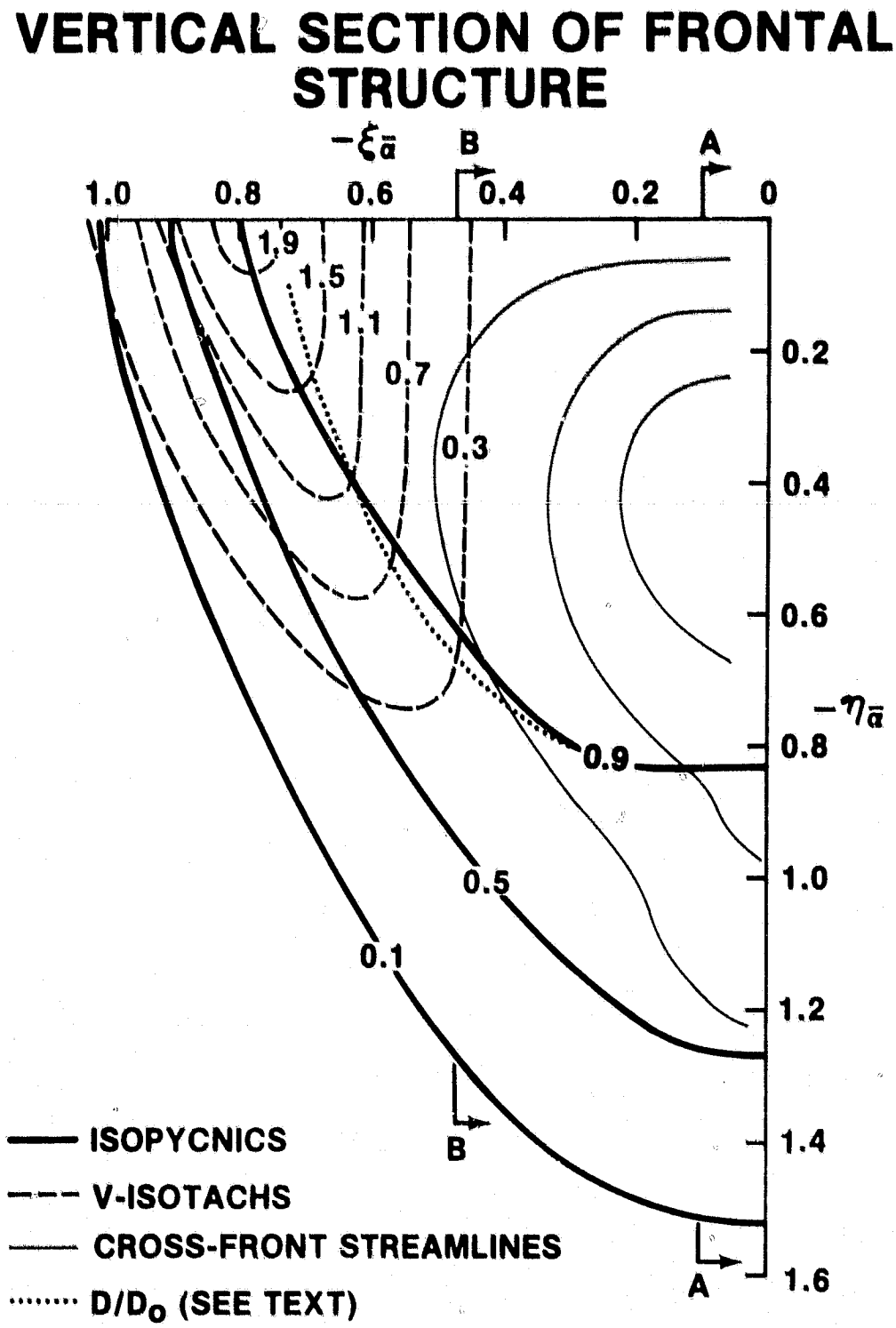

Figure 4. Vertical Section of Frontal Structure at Quasi-steady State.

welling and return flow at greater depths. It should be pointed out that in the quasi-steady state, the front is still undergoing inertial period oscillations, though of small amplitude. The relative streamline pattern in Figure 4 therefore changes over the period and so does the relative cross-front velocity ($\tilde{u} - \tilde{u}_f$) even when the isopycnics and along-front velocity structures are essentially unchanged. In any case, the relative cross-front velocities are typically 1/10 of U_d and the down-welling velocities are more than $(\tilde{R}o)^{-1}$ times smaller. Thus w^* is 10^{-4} to 10^{-3} times the typical along-front surface geostrophic current. The features of the along-front jet and the density anomaly will now be examined in more detail.

Figure 5(a) shows the shape of the horizontal surface manifestation of the along-front jet. The jet is compact with a sharp peak at $\xi_{\tilde{\alpha}} = -0.8$ and is directed Northwards if the light water pool lies to the East of the front. It exhibits anticyclonic shear East of the front and cyclonic shear in the front itself. The vertical profile of $\tilde{v}$ at location of the horizontal jet maximum is shown in Figure 5(b). The vertical shear in $\tilde{v}$ is strongest under the jet maximum. We also observe from Figure 4 that inside the light pool $\tilde{v}$ does not vary with depth, so that $\frac{\partial \tilde{v}}{\partial \eta}$ is indeed zero there. We therefore expect the potential vorticity to be conserved, which yields, together with geostrophy, a Stommel-type result that $\tilde{v}$ decreases exponentially with distance away from the front inside the light pool, and the depth of the light pool deepens expontentially. Indeed, we find

$$\tilde{v} = \tilde{v}_{max}\, e^{-6(0.74 + \xi_{\tilde{\alpha}})}$$

and

$$D = D_o \left\{ 1 - e^{-6(0.74 + \xi_{\tilde{\alpha}})} \right\}$$

where D_o is the dimensionless asymptotic depth of the light pool ($D_o = D_o^*/h_o$) above the main thermocline, i.e. $D_o = 0.82$ according to Figure 4. The curve for D/D_o is shown by a dotted curve in Figure 4 and the curve for $\tilde{v}/\tilde{v}_{max}$ is shown by a short dashed curve in Figure 5(a). It should be noted that exponential decay of $\tilde{v}/\tilde{v}_{max}$ and the exponential deepening of the light pool is generally faster than, though of the same order as, that of Stommel (1966) for the same density anomaly and the same asymptotic depth. However, more than half of the total transport in the jet now takes place in the front itself, outside the potential vorticity conserving region of the light pool. The

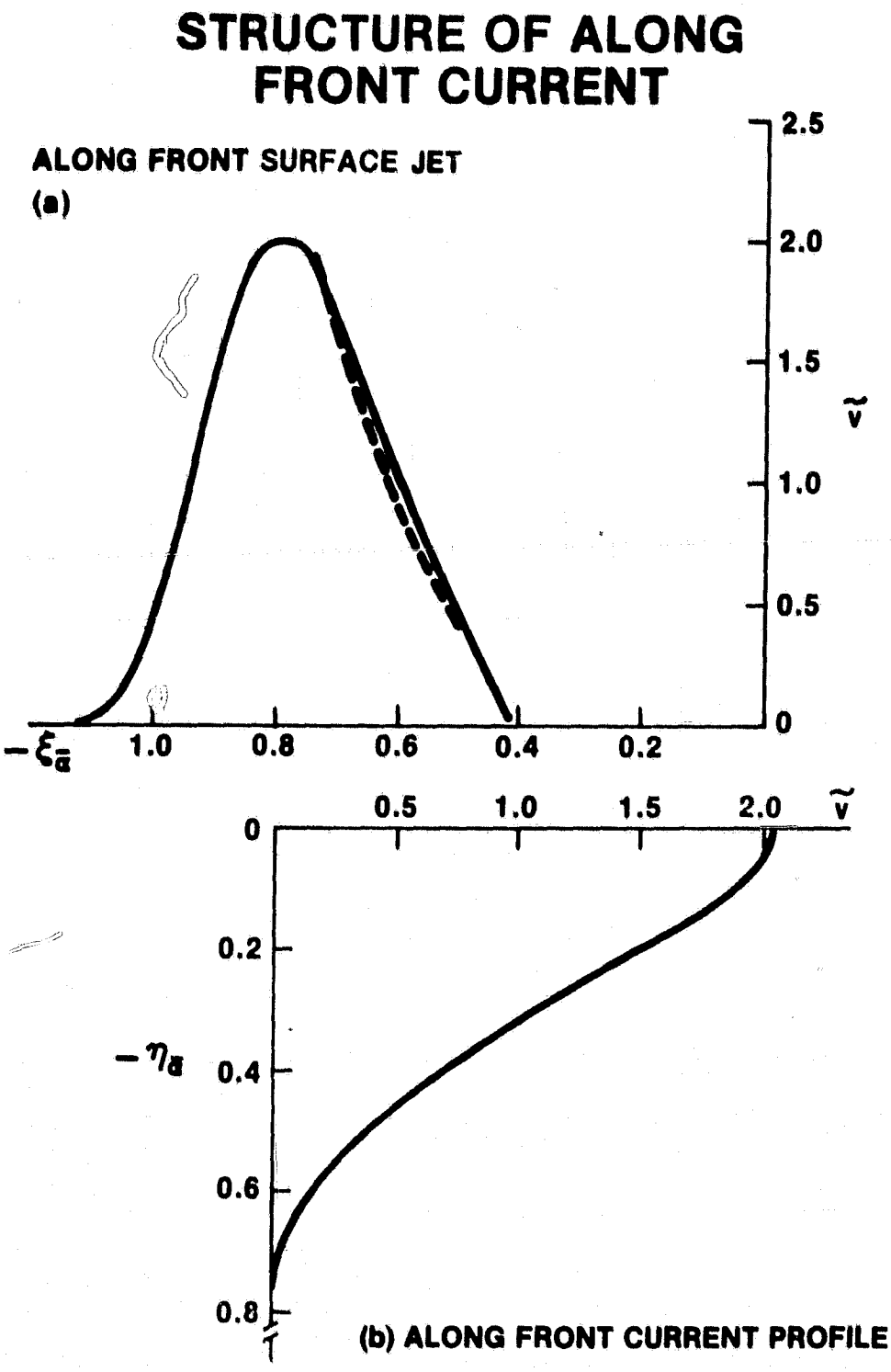

Figure 5. Structure of Along-front Current: (a) Surface jet, (b) vertical profile at jet maximum.

total transport is now found to be equal to 0.38 $g'(D_0^*)^2/f$ compared with a value of $0.5(g' D_0^*)^2/f$ found by Stommel (1966). Although the transport is similar the velocity shear in the along front jet now changes from anticylonic shear in the light pool to cyclonic shear across the front. This feature, together with the conservation of potential vorticity inside the light pool, are benchmarks of success of the present formulation.

Figure 6 shows two density anomaly profiles at station A-A and B-B of Figure 4. The density anomaly exhibits a deep homogeneous layer in the upper part followed by a well-defined thermocline. The profile at A-A gives the thickness of the main thermocline whereas the profile B-B cuts across the sloping isopycnics of the front itself.

Figure 7(a) and (b) show the surface expressions in density and sea-surface height anomalies respectively. The dimensionless sea-surface height anomaly, $\Delta\eta_s$, was found by integrating $\tilde{\gamma}$ vertically. If Δh_s represents the dimensional rise of sea-surface height, then $\Delta\eta_s = (\Delta h_s/\bar{h})\,[\rho_0/(\Delta\rho)_c]$. From the remote sensing, or satellite observational viewpoint, the surface expressions, are rather important manifestations of the frontal structure. It is seen that the surface density anomaly varies more rapidly across the front than the sea-surface height anomaly. The latter varies over the entire width of the frontal region and contains information on the whole vertical cross-sectional structure of the front. The surface density anomaly on the other hand are easily influenced by events that take place in the surface Ekman layer, such as the effect of local wind and local heating and cooling. Thus altimetry data is generally a better indicator of the true location of the front than the infrared data on sea-surface temperature would indicate. The location of the steepest slope of the sea-surface height corresponds rather well with the location of the along-surface current jet maximum. Here again local surface wind effects in the surface Ekman layer has not been included. Local surface wind and heating effects are expected to alter the surface currents and surface temperature and salinity only in the surface Ekman layer. The importance of high quality altimeter data to examine the total depthwise frontal structure cannot be overemphasized. Indeed, given the maximum slope, the total rise height $(\Delta h_s)_{max}$, and the

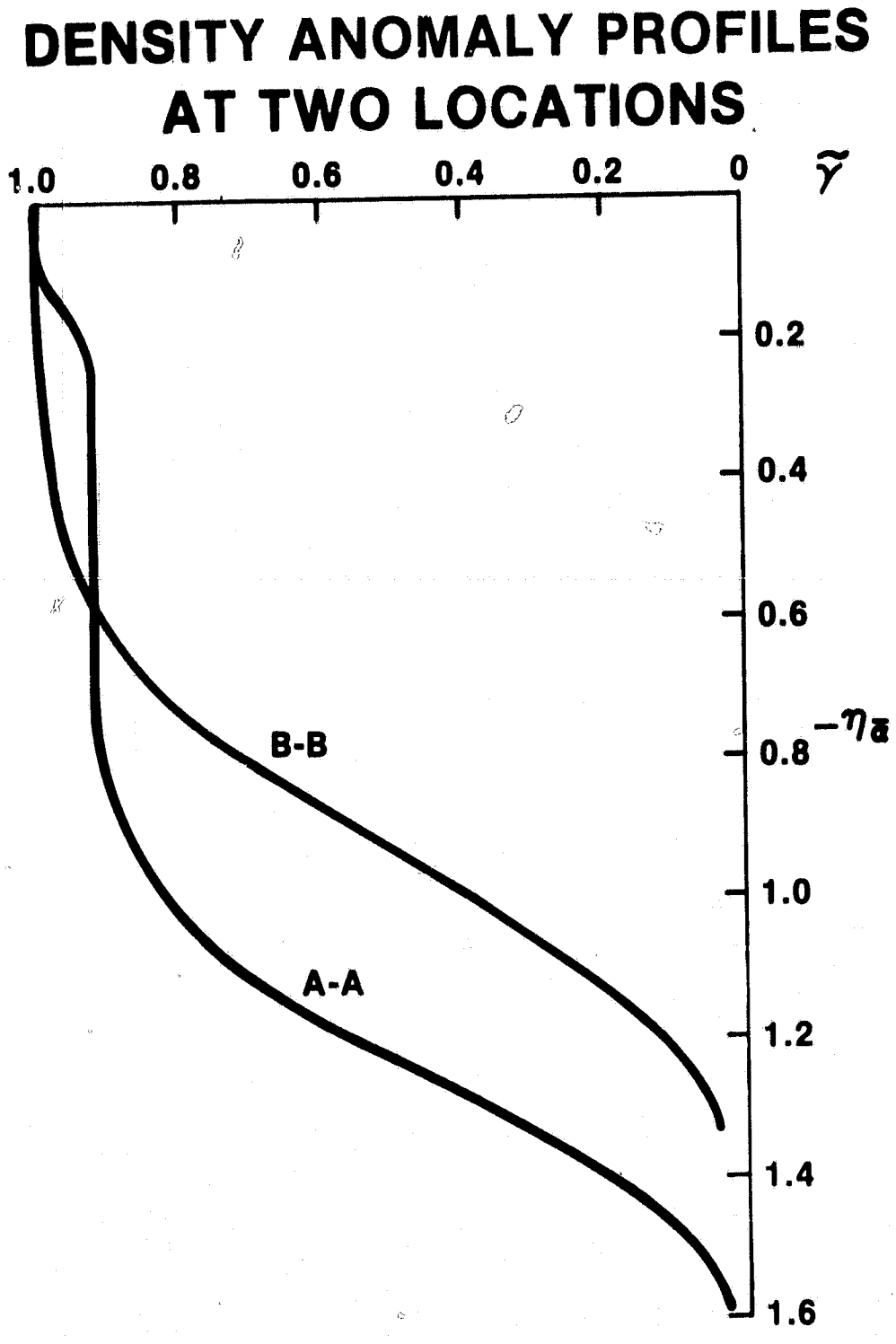

Figure 6. Density Anomaly Profiles at Two Cross-front Locations.

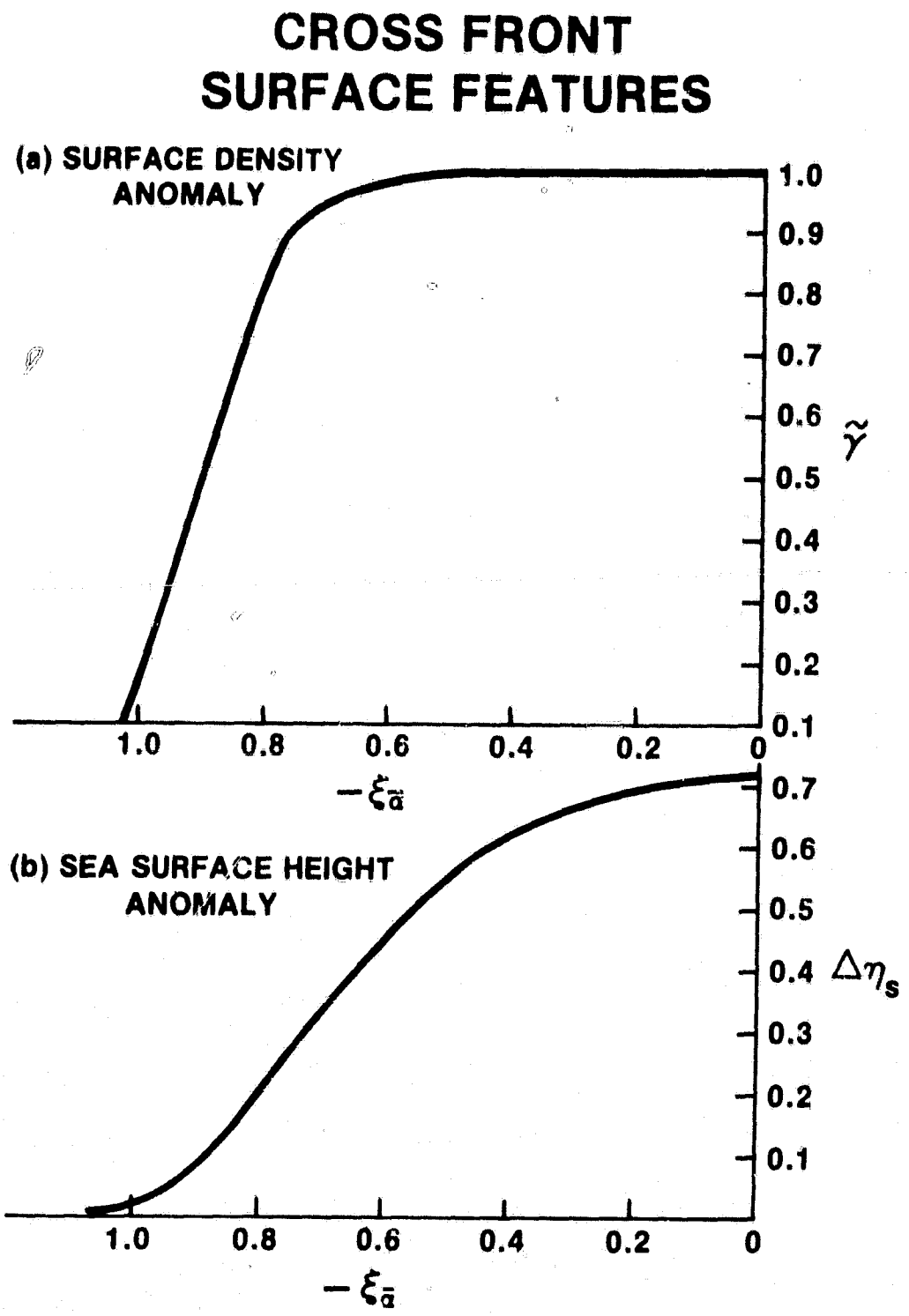

Figure 7. Cross-front Surface Features: (a) density anomaly, (b) sea surface height anomaly.

cross-front width $\bar{L}$ of the sea-surface height anomaly, the hydrography of the front is completely determined according to the present theory.

IV. THE STRUCTURE OF THE GULF STREAM

The results of § III (2) are now applied to study the Gulf Stream. We confine ourself to the upper ocean of approximately 1,500 m or so. The top of the stratified deep ocean serves as a lower boundary of the upper ocean and imposes a limiting depth for the base of the main thermocline. Incorporation of this deep layer and the abyssmal current will be undertaken in a future paper. A few key references on the Gulf Stream should be mentioned: the book by Stommel (1966) and the references cited therein, the article by Fuglister (1963), the monograph by Worthington (1976), and a paper on numerical simulation by Semtner and Mintz (1977).

We may approach the application in the following way. We assume an imposed near surface transport towards the front, i.e. we assume a Q_e, of given density deficit $(\Delta\rho)_e/\rho_o$ relative to the ambient water and examine the structure of the resultant density and flow fields in the quasi-steady state. From the structure, we obtain, in particular, the maximum surface jet velocity v^*_{max}, the mean slope of the inclined isopycnics of the front, the width of the sea surface height anomaly $\bar{L}$ which is the width of the frontal region, the maximum sea surface height anomaly $(\Delta h_s)_{max}$, and the Gulf Stream transport as functions of g', Q_e, f and the depth of the upper ocean $\bar{h}$. The formulas for these quantities as obtained from the results of § III (2) are summarized in Table II.

For example, we take as an initial condition the inflow water to be Sargasso Sea water with a typical temperature of 20°C and 36.6‰ salinity and the ambient water to be the deep upper North Atlantic water of 5°C and 35.0‰ salinity, so that $\Delta\sigma_t = 1.6$ or $(\Delta\rho)_e/\rho_o = 1.6 \times 10^{-3}$ and $g' = 1.5 \times 10^{-2}$ m/s^2. We take the magnitude of Q_e to be 50 m^2/s and f to be 10^{-4}/s. The reference scales U_d, L_o, and h_o are then 0.91 m/s, 9.1 km, and 55 m respectively so that the densimetric Rossby number $\tilde{R}o = 165$. To obtain the value of E, the Ekman number, we take the vertical eddy viscosity coefficient ν_e to be $\sim 0(10)$ cm^2/s. Then $E \sim 0(10^{-3})$ to $0(10^{-2})$. Published estimates on

Table II.
List of formulas for Gulf Stream hydrography

MAXIMUM GEOSTROPHIC SURFACE CURRENT, $v^*_{max} = 2\,(g'\,Q_e)^{1/3}$	(F1)
FRONTAL SLOPE $= 1.5\,f\,(g')^{-2/3}\,Q_e^{1/3}$	(F2)
WIDTH OF SEA SURFACE HEIGHT ANOMALY, $\bar{L} = \frac{\bar{h}}{1.5}\,f^{-1}\,(g')^{+2/3}\,Q_e^{-1/3}$	(F3)
MAXIMUM SEA SURFACE HEIGHT ANOMALY $= 0.7(g'/g)\,\bar{h}$	(F4)
GULF STREAM TRANSPORT $= 0.253\,(\frac{\bar{h}}{1.5})^2\,\frac{g'}{f} = 0.38\,\frac{g'\,D_e^{*2}}{f}$	(F5)

the magnitude of ν_e is subject to a range of variation, so that a precise specification is not justified, nor is it necessary in the present framework since we have shown the results to be insensitive to changes in E for sufficiently low values of E. On using the formulas listed in Table II, with $\bar{h} =$ 1400 m, we get the maximum along-front Gulf Stream velocity v^*_{max} to be 1.82 m/s, the mean slope of the inclined isopycnics to be 1:110, the width of the sea surface anomaly $\bar{L}$ to be 154 km, the maximum sea surface anomaly $(\Delta h_s)_{max}$ to be 1.57 m and the upper ocean Gulf Stream transport to be 33×10^6 m^3/s. The details of the structural feature are shown in the similarity plot of Figure 4. From this we see that the width of the Gulf Stream itself, i.e. the width of the surface jet, is 108 km and the maximum depth of the 30 cm/s $\bar{v}$ – isotach is 750 m from the surface. The thickness of the main thermocline under the light water pool is 650 m.

Table III shows the various Gulf Stream quantities for different values of Q_e while keeping g', f and $\bar{h}$ the same as in the example. These quantities were calculated using the formulas given in Table II. It is seen that a 15 times increase in Q_e increases the slope and maximum jet velocity by $(15)^{1/3}$ or 2.47 times and decreases the width of the jet and $\bar{L}$ by the same amount. The Gulf Stream transport is of course independent of Q_e as seen from formula (F5) and depends only on $\bar{h}$, g' and f. This must be so since the transport is induced geostrophically from the buoyancy derived pressure gradient. For any Q_e, the Gulf Stream transport is sensitive to changes in $\bar{h}$ and g'.

Table III.
Table of Computed Gulf Stream quantities for different Q_e

Q_e (m^2/s)	INITIAL REFERENCE QUANTITIES			GULF STREAM QUANTITIES				
	U_d (m/s)	L_o (km)	h_o (m)	$\tilde{R}o$	MEAN SLOPE OF FRONT	v^*_{max} (m/s)	WIDTH OF SURFACE JET (km)	WIDTH OF SEA-SURFACE HEIGHT ANOMALY $\tilde{L}$ (km)
10	0.53	5.3	19	279	1:186	1.08	182	260
25	0.72	7.2	35	205	1:136	1.44	136	194
50	0.90	9.0	55	165	1:110	1.80	107	154
75	1.03	10.3	73	142	1:95	2.06	94	134
100	1.14	11.4	88	129	1:86	2.28	85	121
125	1.23	12.3	102	120	1:80	2.46	79	113
150	1.30	13.0	115	113	1:75	2.60	74	105

Thus, for comparison with Stommel's (1966) result, taking the depth of the homogeneous light pool to be 800 m and g' to be 2×10^{-2} m/s^2 as used by Stommel (1966), we get a value for the transport of about 50×10^6 m^2/s. The values given for the Gulf Stream quantities in Table III are all accessible to the Stream. This then suggests wide variations of Q_e. Indeed variations of Q_e by several times is reasonable from considering time-dependent variations of wind-driven contribution alone. In addition, there is possibly a significant contribution from the Gulf Stream return flow as described by Worthington (1976).

In the present framework, we now see that the Gulf Stream dynamics is maintained by the near surface shoreward transport of light Sargasso Sea water. The Gulf Stream is a natural geostrophic response to the pressure gradient associated with this buoyant transport. However, at any typical section, say at Cape Fear, the lateral or cross-front forcing induces a geostrophic Gulf Stream transport which is fed by water from further upstream, i.e. from the South. The composition of the water in the Gulf Stream therefore reflects its tropical orgin. Between two neighboring sections, say between Woods Hole and Hatteras, the increase in Gulf Stream transport, if

any, must be contributed by entraining water between the two sections from the Sargasso Sea which is the parent pool of light water. This concept appears to be compatible with the tight re-circulation pattern of the Gulf Stream proposed by Worthington (1976). Finally, it should be pointed out that the formation of the Sargasso Sea warm lens is perhaps partly wind-driven as shown by Semtner and Mintz (1977), but its study belongs to the study of larger scale events and is beyond the scope of the study of frontal dynamics of the present paper.

ACKNOWLEDGEMENTS

This work was done while the author was in the Goddard Laboratory for Atmospheric Sciences, Goddard Space Flight Center, NASA, while on sabbatical leave. The author wishes to thank Dr. David Atlas and Dr. Vincent V. Salomonson for their hospitality and Richard Barbieri, Dr. James Mueller, and Dr. Paul Schopf for many useful discussions. The author is especially grateful to Dr. Mueller for arranging the sabbatical and providing the environment to make it fruitful. The partial support of the National Science Foundation under Grant OCE 77-07953 is also sincerely acknowledged.

REFERENCES

Charney, J. G., 1955: The Gulf Stream as an inertial boundary layer. Proc. Nat. Acad. Sci. U.S., 41, 83-92.

Fuglister, F. C., 1963: Gulf Stream'60, in Progress in Oceanography, Vol. 1, ed. by M. Sears, Macmillan, N.Y.

Garvine, R. W., 1974: Dynamics of small scale oceanic fronts. J. Phys. Oceanogr., 4, 557-569.

Garvine,,R. W., 1979: An integral, hydrodynamical model of upper ocean frontal dynamics: Part I Development and Analysis. J. Phys. Oceanogr., 9, 1-18.

Garvine, R. W., and J. D. Monk, 1974: Frontal structure of a river plume. J. Geophys. Res., 79, 2251-2259.

Kao, T. W., C. Park and H.-P. Pao, 1977: Buoyant surface discharge and small-scale oceanic fronts: A numerical study. J. Geophys. Res., 82, 1747-1766.

Kao, T. W., C. Park and H.-P. Pao, 1978a: Inflows, density currents and fronts. Phys. Fluids, 21, 1912-1922.

Kao, T. W., H.-P. Pao and C. Park, 1978b: Surface intrusions, fronts, and internal waves: A numerical study. J. Geophys. Res., 83, 4641-4650.

Morgan, G. W., 1956: On the wind driven ocean circulation. Deep-Sea Res., 10, 735-748.

Semtner, A. J. and Y. Mintz, 1977: Numerical stimulation of the Gulf Stream and mid-ocean eddies. J. Phys. Oceanogr. 7, 208-230.

Stommel, H., 1966: The Gulf Stream. University of California Press, Berkeley.

Worthington, L. V., 1976: On the North Atlantic circulation. No. 6. The Johns Hopkins Oceanographic Studies, The Johns Hopkins Univ. Press. Baltimore and London.

APPENDIX A

In the formulation given in III, the region of integration has a finite depth d. For the sake of computational convenience, d is used as the reference length, Q_e/d as the reference velocity and d^2/Q_e as the reference time in that scheme. The dimensionless parameters are $Ro = U/(fd)$, $Re = Ud/\nu_e$, $F = U/(gd)^{1/2}$ and $F_e = 10^{3/2}\, F/\gamma_e^{1/2}$. The conversions of the computer results to the present normalization is achieved by the following formulas:

$$\xi = (10\,Ro)^{-1}\, F_e^{2/3}\, x \qquad (A1)$$

$$\eta = 10\, F_e^{-2/3}\, z \qquad (A2)$$

$$\tilde{u} = (10)^{-1}\, F_e^{2/3}\, u \qquad (A3)$$

$$\tilde{w} = 10\, Ro\, F_e^{-2/3}\, w \qquad (A4)$$

$$\tau = (Ro)^{-1}\, t \qquad (A5)$$

$$\tilde{Ro} = 100\, Ro/F_e^{4/3} \qquad (A6)$$

$$E = 100\, Ro/(Re\, F_e^{4/3}) \qquad (A7)$$

$$h_o/d = (10^{-1})\, F_e^{2/3} \qquad (A8)$$

APPENDIX B

If we normalize the governing equations by the buoyancy velocity, length and time scales, the equations corresponding to (3), (5), (6) and (7) are

$$\tilde{\zeta} = \nabla^2 \tilde{\Psi} \tag{B1}$$

$$\frac{\partial \tilde{\gamma}}{\partial t_1} + \frac{\partial}{\partial \xi_1}(\tilde{u}\,\tilde{\gamma}) + \frac{\partial}{\partial \eta}(\tilde{w}_1\,\tilde{\gamma}) = \frac{1}{Re}\nabla^2 \tilde{\gamma} \tag{B2}$$

$$\frac{\partial \tilde{\zeta}}{\partial t_1} + \frac{\partial}{\partial \xi_1}(\tilde{u}\,\tilde{\zeta}) + \frac{\partial}{\partial \eta}(\tilde{w}_1\,\tilde{\zeta}) - \frac{1}{\tilde{R}o}\frac{\partial \tilde{v}}{\partial \eta} = \frac{\partial \tilde{\gamma}}{\partial \xi_1} + \frac{1}{Re}\nabla^2 \tilde{\zeta} \tag{B3}$$

$$\frac{\partial \tilde{v}}{\partial t_1} + \frac{\partial}{\partial \xi_1}(\tilde{u}\,\tilde{v}) + \frac{\partial}{\partial \eta}(\tilde{w}_1\,\tilde{v}) + \frac{1}{\tilde{R}o}\,\tilde{u} = \frac{1}{Re}\nabla^2 \tilde{v} \tag{B4}$$

where $\xi_1 = x^*/h_o$, $t_1 = t^*/T_1$, $w_1 = \tilde{w}^*/U_d$ $\nabla^2 \equiv \frac{\partial^2}{\partial \xi_1^2} + \frac{\partial^2}{\partial \eta^2}$.

In the non-rotating limit $\tilde{R}o = \infty$, (B4) is uncoupled from the other equations, and is identically zero for an initial value problem starting from rest. The steady-state is approached for $t_1 \to \infty$, $\tau = 0$. For $\tilde{R}o \neq \infty$ however, the steady-state is approached for $t_1 \to \infty$ and τ large. The approach to steady-state is thus not uniform for $\tilde{R}o \to \infty$. Hence the limit $t_1 \to \infty$ and $\tilde{R}o \to \infty$ are not interchangeable.